https://doi.org/doi:10.1093/plphys/kiab504 PLANT PHYSIOLOGY 2022: 188: 97–110

Plant Physiology®

Breakthrough Tech

Spatio-temporal strigolactone signaling patterns in intact plants

Changzheng Song,[1] Jiao Zhao,[1] Marjorie Guichard ,[1,2] Dongbo Shi ,[1,3] Guido Grossmann ,[1,2] Christian Schmitt ,[1,†] Virginie Jouannet [1] and Thomas Greb [1,*,‡]

1 Centre for Organismal Studies (COS), Heidelberg University, Im Neuenheimer Feld 360, 69120 Heidelberg, Germany
2 Institute of Cell and Interaction Biology, Heinrich-Heine-University Düsseldorf, Universitätsstraße 1, 40225 Düsseldorf, Germany
3 RIKEN Center for Sustainable Resource Science (CSRS), 1-7-22 Suehiro-cho, Tsurumi-Yokohama 230-0045, Japan

*Author for communication: thomas.greb@cos.uni-heidelberg.de
†Present address: Institute of Pharmacy and Molecular Biotechnology, Im Neuenheimer Feld 364, 69120 Heidelberg, Germany.
‡Senior author.
These authors contributed equally (C.So., J.Z.).
C.So., J.Z., M.G., D.S., C.S., and V.J. designed and conducted the experiments. C.So, G.G., J.Z., and T.G. conceptualized the experiments. C.So. and T.G. wrote the manuscript.
The author responsible for distribution of materials integral to the findings presented in this article in accordance with the policy described in the Instructions for Authors (https://academic.oup.com/plphys/pages/general-instructions) is: Thomas Greb (thomas.greb@cos.uni-heidelberg.de).

Abstract

Strigolactones (SLs) are a class of plant hormones that mediate biotic interactions and modulate developmental programs in response to endogenous and exogenous stimuli. However, a comprehensive view on the spatio-temporal pattern of SL signaling has not been established, and tools for a systematic in planta analysis do not exist. Here, we present Strigo-D2, a genetically encoded ratiometric SL signaling sensor that enables the examination of SL signaling distribution at cellular resolution and is capable of rapid response to altered SL levels in intact Arabidopsis (*Arabidopsis thaliana*) plants. By monitoring the abundance of a truncated and fluorescently labeled SUPPRESSOR OF MAX2 1-LIKE 6 (SMXL6) protein, a proteolytic target of the SL signaling machinery, we show that all cell types investigated have the capacity to respond to changes in SL levels but with very different dynamics. In particular, SL signaling is pronounced in vascular cells but low in guard cells and the meristematic region of the root. We also show that other hormones leave Strigo-D2 activity unchanged, indicating that initial SL signaling steps work in isolation from other hormonal signaling pathways. The specificity and spatio-temporal resolution of Strigo-D2 underline the value of the sensor for monitoring SL signaling in a broad range of biological contexts with highly instructive analytical depth.

Introduction

Strigolactones (SLs), a class of carotenoid-derived phytohormones, were originally identified in plant root exudates acting as germination stimulants for parasitic plants (Cook et al., 1966). Since then, an increasing number of roles of SLs as stimulants of biotic interactions (Akiyama et al., 2005) and as endogenous growth regulators in a broad range of species has been unveiled. The spectrum of SL-dependent processes includes the determination of root architecture, shoot branching, radial growth, leaf development, flower size, and the adaptation to drought and nutrient availability (Gomez-Roldan et al., 2008; Al-Babili and Bouwmeester, 2015; Yang et al., 2019; Chesterfield et al., 2020), which makes SL biology a highly relevant topic for exploring and modifying plant performance. In spite of this broad spectrum of SL-dependent processes and the role of SLs in long-distance communication (Wheeldon and Bennett, 2021), knowledge about SL distribution and the pattern of SL signaling with high spatial resolution is surprisingly scarce.

Biosynthesis of SLs is initiated by converting all-trans-β-carotene to 9-cis-β-carotene through the all-trans/9-cis-carotene isomerase DWARF27 (D27). The 9-cis-β-carotene is then sequentially converted by CAROTENOID CLEAVAGE

Received August 06, 2021. Accepted October 09, 2021. Advance access publication October 29, 2021

DIOXYGENASE 7 (CCD7) and CCD8 homologs into carlactone, which is the last common biosynthetic precursor for all known SLs (Alder et al., 2012; Seto et al., 2014). The downstream biosynthetic pathways leading to functional SLs vary among species, resulting in species-specific SL repertoires (Zhang et al., 2014; Brewer et al., 2016; Waters et al., 2017). In all cases, however, canonical SLs carry a butenolide ring (D-ring) linked to a less conserved tricyclic lactone (the ABC rings) via an enol-ether bond (Wang and Bouwmeester, 2018; Yoneyama et al., 2018). Based on stereochemical differences at the junction of the B and C rings, SLs are divided into strigol- and orobanchol-like subfamilies, exemplified by 5-deoxystrigol and 4-deoxyorobanchol, respectively. In addition to canonical SLs, there are compounds with SL-like activity lacking the B- and C-rings such as methyl carlactonoate and heliolactone (Wang and Bouwmeester, 2018; Yoneyama et al., 2018). Overall, at least 25 different compounds with SL-like activity have been discovered in plants all exhibiting a 2′R configuration in the D-ring (Wang and Bouwmeester, 2018). Importantly, grafting experiments and gene expression analyses indicate that SLs are synthesized in both roots and shoots (Booker et al., 2005; Domagalska and Leyser, 2011; Ruyter-Spira et al., 2013) but can be transported long distances, possibly along the vasculature (Kohlen et al., 2011).

In Arabidopsis (*Arabidopsis thaliana*), similarly as in other species, bioactive SL molecules are perceived by homologs of the nuclear α/β-hydrolase superfamily protein DWARF14 (D14; Arite et al., 2009; Waters et al., 2012; Seto et al., 2019). Although still being controversial in some details, the current view is that D14 proteins fulfill roles as both SL receptors and as enzymes that cleave and deactivate SL molecules (Shabek et al., 2018; Seto et al., 2019). In any case, binding of SLs to D14 induces conformational changes in the D14 structure and its recruitment to an Skp, Cullin, F-box (SCF) E3 ubiquitin–protein ligase complex, containing the F-box protein MORE AXILLARY GROWTH 2/DWARF3 (MAX2/D3; Yao et al., 2016; Shabek et al., 2018; Seto et al., 2019). MAX2/D3 serves as an adapter providing specificity toward the recruitment of D14 and, upon D14 binding, also recruits proteins from the SUPPRESSOR OF MAX2 1-LIKE/DWARF53 (SMXL/D53) family, in particular SMXL6, SMXL7, and SMXL8 (Soundappan et al., 2015; Wang et al., 2015). After formation of an $SCF^{MAX2/D14/SMXL}$ complex, SMXL proteins are polyubiquitinated and degraded by the cellular proteasome—the decisive step for modulating SL-dependent processes (Jiang et al., 2013; Zhou et al., 2013).

MAX2 is broadly expressed in the seedling stage, but is expressed predominantly in vascular tissues and meristems at adult stages (Shen et al., 2007; Stirnberg et al., 2007; Wendrich et al., 2020). *D14* expression patterns largely overlap with those of *MAX2* (Chevalier et al., 2014; Wendrich et al., 2020) allowing physical interactions between these proteins and SL signaling in the nuclei of respective cells. Therefore, based on expression analyses of key signaling components, differences in the potential of different cell types to perceive and to transmit SL signals is likely. However, differences in signaling capacities among cell types and growth stages have not been investigated systematically so far.

Of note, the Arabidopsis KARRIKIN-INSENSITIVE2 (KAI2) protein, a homolog of D14, mediates signal transduction of smoke-derived karrikin (KAR) molecules via a comparable SCF complex-based mechanism and, most likely, serves as a receptor for a yet to be identified endogenous signaling molecule (Waters et al., 2012, 2017; Zhao et al., 2013; Conn and Nelson, 2015; Soundappan et al., 2015). Similar to the interactions between D14 and MAX2 in SL signaling, MAX2 is responsible for recruiting KAI2 after KAR binding. Instead of SMXL6, SMXL7 and SMXL8, however, it is predominantly the SMXL family proteins SUPPRESSOR OF MAX2 1 (SMAX1) and SMXL2 that are targeted by KAR signaling (Soundappan et al., 2015; Stanga et al., 2016; Khosla et al., 2020a). With regard to the specificity of the SL and KAR signaling pathways, it is important to be aware that synthetic SL analogs do not only hold a 2′R configuration but also an enantiomeric 2′S configuration and that the latter have the potential to activate KAI2 (Flematti et al., 2016; Li et al., 2016). Therefore, the sharing of components between the SL and KAR signaling pathways and a lack of specificity of some synthetic hormone analogs makes it sometimes challenging to determine the effect of each pathway individually.

As key mediators of SL responses, nuclear SMXL/D53 proteins are predicted to contain an N-terminal double Clp-N domain (D1) and one or two P-Loop NTPase domains (D2, Figure 1A; Moturu et al., 2018; Shabek et al., 2018). Although their exact mode of action in the nucleus is unclear, SMXL6, SMXL7, and SMXL8 proteins show DNA binding capabilities in vitro and in planta and determine the activity of decisive regulatory genes, for example *BRANCHED1* (*BRC1*) in the context of shoot branching (Wang et al., 2020). Importantly, previous research by Shabek et al. (2018) showed that the D2 domain of the rice (*Oryza sativa*) D53 protein alone forms a stable complex with D14–D3–ASK1 proteins and is also degraded by the proteasome in a MAX2/D3-dependent manner. This indicates that the D2 domain is sufficient for hormone-induced and $SCF^{MAX2/D14}$-catalyzed protein turnover.

Genetically encoded fluorescent biosensors are versatile tools for detecting changing levels of small molecules in vivo (Uslu and Grossmann, 2016; Isoda et al., 2021). Due to the unsurpassed capability of revealing relative molecule levels with high spatio-temporal resolution and within a physiological range, sensors have been developed for measuring small molecules like calcium, sugars, and various plant hormones (Miyawaki et al., 1997; Fehr et al., 2002; Takanaga et al., 2008; Waadt et al., 2014; Larrieu et al., 2015). In previous SL studies, ratiometric biosensors were used to exploit the levels of the SMXL6 or SMXL7 proteins to characterize the activity of the SL signaling pathway (Samodelov et al., 2016; Khosla et al., 2020a, 2020b; Braguy et al., 2021). The sensors responded, as expected, to various natural or synthetic SLs with high specificity, sensitivity, and quantitative resolution,

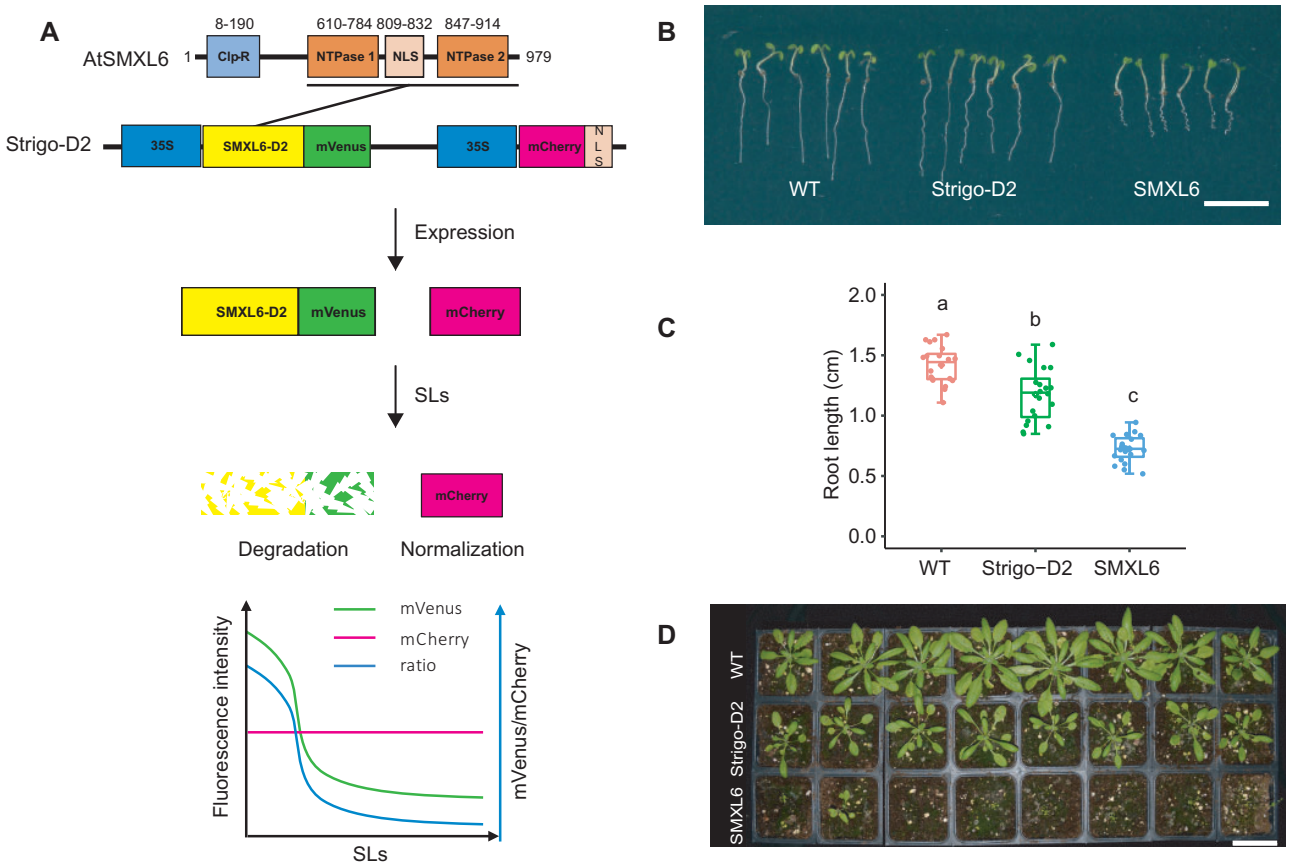

Figure 1 Sensor construction and phenotypic analysis of Strigo-D2 lines. A, Schematic representation of the SMXL6 protein domain structure and the Strigo-D2 design. Numbers above domains represent amino acid positions. The D2 domain ranges from 615 to 979 aa. SL: strigolactone. B–D, Phenotypes of transgenic plants expressing SMXL6-D2-mVenus ("Strigo-D2", shown is Line 1 mentioned in Figure 2) and SMXL6-mVenus ("SMXL6") in comparison to WT plants. B, Seedlings five days after germination. C, Root length quantification of 5-d-old seedlings. Elements of the boxplot: center line, median; box limits, upper and lower quartiles; whiskers, values outside upper and lower quartiles; end of the whiskers, minimum and maximum. Each dot represents the value of one biological replicate as described in the methods section. Different letters above boxes indicate statistical groups (one-way analysis of variance (ANOVA), post hoc LSD test with Bonferroni adjustment, $P < 0.0001$, $n = 20$). D, Plants four weeks after germination. Scale bars: 1 cm (B) or 5 cm (D).

demonstrating the suitablity of using proteolytic targets of the SL signaling pathway to estimate respective signaling levels. However, some of the described sensors use bioluminescence as a readout, hampering cellular imaging and requiring continuous supply of luciferin, the substrate of the luciferase reporter (Samodelov et al., 2016; Khosla et al., 2020a; Braguy et al., 2021). Moreover, ratiometric SL sensors have only been tested successfully in transient expression systems so far (Samodelov et al., 2016; Khosla et al., 2020a, 2020b; Braguy et al., 2021), leaving open the question of their performance in stable transgenic plant lines and in the context of an SL-controlled process. In comparison, a sensor stably integrated in plants expressing the luminescently labeled D2 domain of SMAX1 under the control of the ubiquitously active *UBQ10* promoter was recently shown to faithfully report KAR signaling (*pRATIO2251-SMAX1*$_{D2}$; Khosla et al., 2020b). Demonstrating the challenges of these approaches, a fluorescent reference protein supposedly co-translated with the same sensor could not be detected, preventing normalization of sensor activity (Khosla et al., 2020b).

Here, we present the fluorescent ratiometric biosensor Strigo-D2, which allows semi-quantitative monitoring of SL signaling levels with cellular resolution in intact Arabidopsis plants (Figure 1A). Strigo-D2 employs ubiquitous expression of the SMXL6 D2 domain fused to the yellow fluorescent protein mVenus to reveal the capacity of cells to proteolytically degrade SL signaling targets. SMXL6-D2-mVenus levels are directly compared to levels of the red fluorescent protein mCherry expressed under the control of the same ubiquitously active promoter from the same transgene allowing convenient normalization of signal intensities.

Results

Strigo-D2-plants show only mild growth alterations

To test the capacity of the SMXL6 protein to serve as an in planta-SL signaling sensor, we generated plant lines expressing full length SMXL6 or only the SMXL6-D2 domain fused to the yellow fluorescent mVenus protein (Kremers et al., 2006) under the control of the broadly active *35S* promoter

(Benfey and Chua, 1990). In addition, the lines expressed a *35S*-driven nuclear-localized version of mCherry (Shaner et al., 2004; mCherry-NLS) from the same transgene to normalize signal intensities (Figure 1A). Comparing transgenic plants with wild-type (WT) revealed that plants expressing the full SMXL6-mVenus fusion protein showed much shorter roots at the seedling stage and substantially retarded growth as adults (Figure 1, B–D), suggesting a severe interference of the broadly expressed SMXL6 protein with endogenous regulatory processes. Instead, roots of SMXL6-D2 expressing plants were only slightly shorter than WT roots and growth was more similar to WT overall (Figure 1, B–D). When comparing fluorescence intensities, strong mCherry but only weak mVenus-derived signals were detected in nuclei of *p35S:SMXL6-mVenus_p35S:mCherry-NLS* seedlings expressing the full length SMXL6-mVenus protein using standard microscopy settings (Supplemental Figure S1). In comparison, *p35S:SMXL6-D2-mVenus_p35S:mCherry-NLS* seedlings expressing SMXL6-D2-mVenus showed a clear nuclear mVenus signal when applying low laser intensity (Supplemental Figure S1).

Consistent (+)-5DS response in independent Strigo-D2 lines

Due to the mild effect of SMXL6-D2 on plant growth in comparison to the full-length protein and the robust detection of SMXL6-D2-mVenus fluorescence, we decided to explore whether SMXL6-D2-expressing plants are able to faithfully report on internal SL signaling levels. To this end, three independent transgenic SMXL6-D2 lines were treated with 0.5-µM (+)-5-deoxystrigol ((+)-5DS), which induces SL signaling (Scaffidi et al., 2014; Samodelov et al., 2016; Villaécija-Aguilar et al., 2019). In nuclei of the root maturation zone, a substantial reduction of the mVenus/mCherry intensity ratio was observed 20 min after application; the ratio continued to decrease for at least 1 h (Figure 2, A–F). This indicated, as expected, a negative correlation between the mVenus/mCherry intensity ratio and the level of SL signaling. Changes in intensity ratios were solely dependent on a reduction of SMXL6-D2-mVenus levels as mCherry-derived signals were fully stable over time. These results demonstrated that, although initial levels were higher than the full SMXL6-mVenus protein, the SMXL6-D2-mVenus protein responded to a pharmacological activation of SL signaling with similar dynamics as previously reported for fluorescently labeled full length SMXL/D53 proteins (Zhou et al., 2013; Soundappan et al., 2015; Wallner et al., 2017). Moreover, mCherry-NLS signals appeared to be a suitable reference for determining SL-dependent alterations in SMXL6-D2-mVenus levels. When comparing SMXL6-D2-mVenus signal dynamics among the three lines, line 1 showed the largest dynamic range over the incubation period (Figure 2, A–F) prompting us to perform subsequent analyses taking advantage of the transgene present in this line. Expecting that the SMXL6-D2-mVenus/mCherry intensity ratio is tightly correlated with SL signaling levels, we named the sensor "Strigo-D2" from here on.

The Strigo-D2 response depends on the SL signaling pathway

Dose-response analyses in root maturation zones showed that Strigo-D2 responded to concentrations as low as 5-nM (+)-5DS and that the response curve started to flatten at 0.5-µM (+)-5DS (Figure 3A), demonstrating high sensor sensitivity. To confirm whether Strigo-D2 specifically reports on SL signaling, we treated Strigo-D2 plants for two hours with 0.5 µM (+)-5DS, *rac*-GR24, $GR24^{4DO}$, or KAR1 (Scaffidi et al., 2014). As a result, a clear response was observed when applying the SL signaling inducers (+)-5DS, *rac*-GR24, and $GR24^{4DO}$ but not when applying KAR1 which specifically induces KAR signaling (Scaffidi et al., 2014; Villaécija-Aguilar et al., 2019; Figure 3B; Supplemental Figure S2). In comparison, treating *d14* mutants carrying the same transgene had no effect on Strigo-D2 activity, whereas the sensor responded similarly in the WT and the *kai2* mutant backgrounds (Figure 3B; Supplemental Figure S2). These results let us conclude that Strigo-D2 specifically responded to SL signaling and that this effect was fully dependent on the SL receptor D14. In this context, it is important to note that *rac*-GR24 and (+)-5DS activate both strigolactone and karrikin signaling pathways whereas $GR24^{4DO}$ specifically induces SL signaling (Scaffidi et al., 2014; Villaécija-Aguilar et al., 2019). We could confirm this distinction by treating an *pSMXL5:SMAX1-Venus* reporter line revealing KAR signaling responses (Wallner et al., 2017), which responded to (+)-5DS, *rac*-GR24, and KAR1 but not $GR24^{4DO}$ (Supplemental Figure S3). Further supporting specificity of Strigo-D2 in reporting SL signaling levels, the phytohormones 3-indoleacetic acid (IAA), trans-Zeatin, abscisic acid (ABA), and gibberellic acid (GA_3), had no effect on sensor activity after 2 h of exposure (Figure 3C; Supplemental Figure S4). In summary, Strigo-D2 showed an SL-specific response, indicating that it is reliable for analyzing SL signaling at cellular resolution.

Strigo-D2 shows cell type-specific activity patterns

To explore the potential of Strigo-D2 to reveal spatial patterns of SL-signaling, tile scanning of whole Strigo-D2 seedlings was performed, revealing the activity pattern of Strigo-D2. As expected, signals of mVenus and mCherry were detected throughout 4-d-old seedlings, reflecting the ubiquitous expression of Strigo-D2 under the control of the *35S* promoter (Figure 4, A–E; Supplemental Figure S5). Interestingly, different intensity ratios of mVenus and mCherry fluorescence among tissues were found, with ratios in meristematic and elongation zones of root tips being higher than those in root maturation zones and hypocotyls (Figure 4, F–J; Supplemental Figure S5). Intensity ratios were especially high in stomata guard cells, which differed substantially from other epidermal cells in this regard (Figure 4, F and J). In contrast, vascular cells displayed a low intensity ratio in all organs tested (Figure 4, G and J; Supplemental

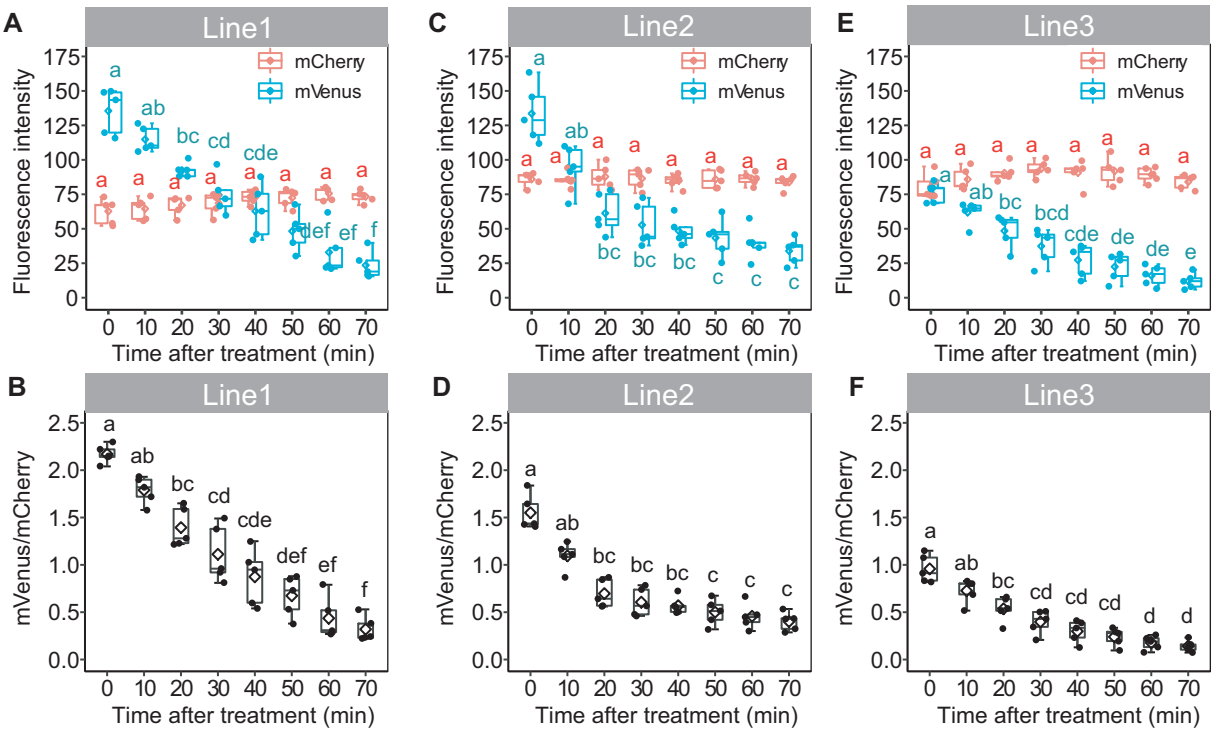

Figure 2 Strigo-D2 response to (+)-5DS in three independent transgenic lines. A–F, Fluorescence intensity of mVenus and mCherry (A, C, and E) and mVenus/mCherry signal ratios (B, D, and F) in the root maturation zone upon treatment with 0.5 μM of (+)-5DS are shown for line 1 (A and B), line 2 (C and D), and line 3 (E and F). Elements of the boxplot: center line, median; box limits, upper and lower quartiles; whiskers, values outside upper and lower quartiles; end of the whiskers, minimum and maximum. Each dot represents the value of one biological replicate as described in the "Materials and Methods" section. Different letters above boxes indicate statistical groups (one-way ANOVA, post hoc LSD test with Bonferroni adjustment, $p < 0.01$, $n = 5$).

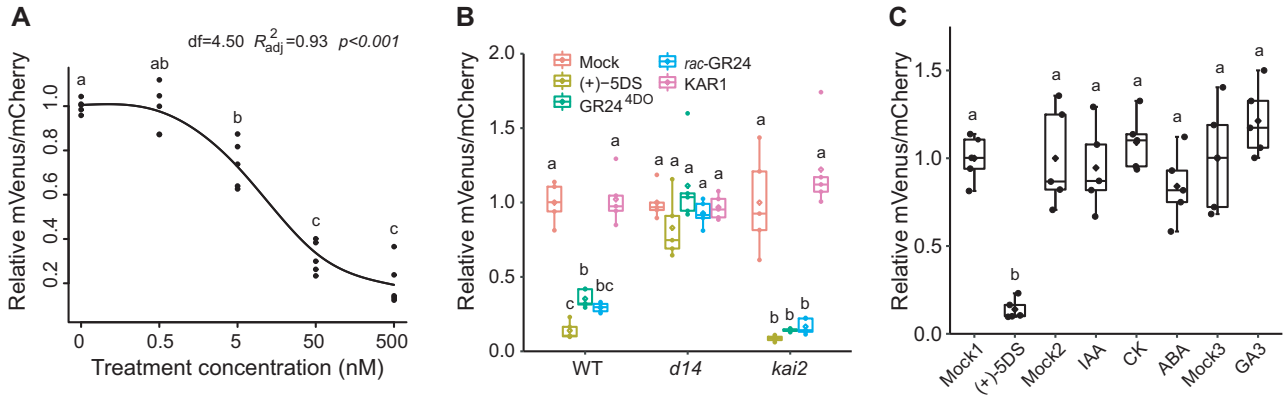

Figure 3 Specificity of Strigo-D2 in responding to the SLs signaling pathway. A) Dose–response of Strigo-D2 to (+)-5DS treatment in root maturation zone. Treatment duration was 60 min. The curve was generated by nonlinear regression and computed in R using the ss Function in the npreg Package. df: degree of freedom. Shown are the values of five biological replicates. Adjusted R square indicates how well generated curves fit obtained data points. *P*-value for the *F* test indicates significance level of the correlation between the model and obtained data. B, Responses of Strigo-D2 in the root maturation zone of different genetic backgrounds (WT, *d14*, *kai2*) to various SL molecules and to KAR1. C, Responses of Strigo-D2 in the root maturation zone to other plant hormones (IAA, CK, ABA, or GA_3). Mock1: treatment with (+)-5DS solvent. Mock2: treatment with the solvent for IAA, CK, and ABA solvent. Mock3: treatment with the solvent for GA_3. Elements of the boxplot: center line, median; box limits, upper and lower quartiles; whiskers, values outside upper and lower quartiles; end of the whiskers, minimum and maximum. Letters above the curve or boxes indicate statistical groups (one-way ANOVA, post hoc LSD test with Bonferroni adjustment, $P < 0.01$, $n = 5$).

Figure S6), which is in line with the reported vascular-associated expression of SL signaling components (Stirnberg et al., 2007; Chevalier et al., 2014) and as confirmed by fluorescent *MAX2* and *D14* promoter reporters (Supplemental Figure S7). Taken together, we concluded that the activity of Strigo-D2 showed cell type-specific signatures and a spatial association of its activity with the expression pattern of SL signaling components.

Strigo-D2 reveals tissue-specific (+)-5DS responsiveness

To explore local specificities of Strigo-D2 dynamics, (+)-5DS was applied to cotyledons, hypocotyls, and the root maturation, elongation, and meristematic zones. In cotyledons, a significant decrease of the mVenus/mCherry ratio was observed 30 min after application, and the ratio continued to decrease to a very low level within 1 h (Figure 5A; Supplemental Movie 1). In comparison, ratio reduction was slower in hypocotyls where a significant decrease was only found 50 min after application (Figure 5B; Supplemental Movie 2). With 20 min after application, the fastest response was found in root maturation zones where the ratio decreased continuously until 70 min after the start of treatment (Figure 5C; Supplemental Movie 3). The sensor responded in a similar manner in root elongation zones, where a notable reduction of mVenus/mCherry ratios was observed at 30 min when ratios started to decrease sharply until reaching a minimum 40 min after application (Figure 5D; Supplemental Movie 4). Interestingly, in the root apical meristem, a significant reduction of the mVenus/mCherry ratio was only found 40 min after (+)-5DS application (Figure 5E; Supplemental Movie 4) arguing for a reduced responsiveness for this tissue. Additionally, spline regression estimating functional relationships between relative mVenus/mCherry intensity ratio and treatment time also statistically verified the different dynamics of the responses comparing different tissues (Supplemental Figure S8). Indeed, when analyzing the root tip with higher spatial resolution along the longitudinal axis, we discovered a gradual decrease of responsiveness going from the maturation zone to the very tip of the root (Figure 6, A and B; Supplemental Figure S9A and Supplemental Movie 5). Along the same lines, application of 0.5- and 0.05-μM (+)-5DS resulted in a similar Strigo-D2 response dynamics in the maturation and elongation zone, but the meristematic zone responded only slightly to 0.05 μM and not at all when adding 0.005-μM (+)-5DS (Figure 7, A–C). This was in contrast to the maturation and elongation zones, which showed at least a slow response to 0.005 μm (+)-5DS (Figure 7, A and B). Regression analysis also showed different dynamics of the response to different (+)-5DS concentrations (Supplemental Figure S10, A–C). These observations argued for a gradient of SL responsiveness in the root with a maximum in mature tissues and decreasing toward non-differentiated tissues along the longitudinal axis. Such a gradient is in line with a predominant expression of *D14* and *MAX2* in mature vascular tissues of the root (Supplemental Figure S7) and the note that at least the D14 protein travels over short distances (Chevalier et al., 2014), potentially generating a concentration gradient of the capacity to perceive SL molecules.

In cotyledons, pavement cells showed a rather fast response to (+)-5DS treatments and a sharp decrease of the mVenus/mCherry ratio. In comparison, the response in guard cells was relatively slow and lasted longer before the ratio reached a minimum level after 90 min (Figure 6, C and D; Supplemental Figure S9B and Supplemental Movie 6). This observation again argued for a cell type-specific SL signaling potential with substantial differences between neighboring cells. Interestingly, whereas transcriptional reporters revealed both *MAX2* and *D14* expression in the cotyledon vasculature, only *D14* expression could be detected in guard cells (Supplemental Figure S7) implying that the a reduced Strigo-D2 response in these cells is particularly due to low levels of *MAX2* activity.

Discussion

Genetically encoded biosensors are powerful tools for analyzing distribution and dynamics of small molecules with minimal invasion and high spatiotemporal resolution. Diverse biosensors for phytohormones or their activity have been successively developed over the past two decades (reviewed in Isoda et al., 2021). However, ratiometric sensors allowing semi-quantitative analysis of strigolactone signaling in intact plants are still missing. As a major target of SL signaling in Arabidopsis, the full length SMXL6 protein has shown rapid *rac*-GR24-induced degradation in previous studies (Wang et al., 2015; Samodelov et al., 2016), with some difficulties to detect a *35S*-driven SMXL6-yellow fluorescent protein (YFP) fusion in more differentiated tissues (Bennett et al., 2016). Similarly, in our study, only weak mVenus signals were detected in transgenic *p35S:SMXL6-mVenus_p35S:mCherry-NLS* seedlings. Moreover, ubiquitous expression of a full SMXL6-mVenus protein had adverse effects on plant development making it unsuitable to serve as an informative readout for strigolactone signaling in a natural context. In comparison, the truncated SMXL6-D2-mVenus protein had milder effects on plant performance, was robustly detected in microscopic analyses and responded specifically to SL-signaling. In particular, D14-deficiency caused insensitivity of SMXL6-D2-mVenus against the pharmacological induction of SL-signaling, whereas KAI2-deficiency had no effect; some cross-reaction of both pathways on the level of the SMXL protein targets has been suggested (Khosla et al., 2020a; Wang et al., 2020). We thus conclude that SMXL6-D2-mVenus levels specifically report on SL signaling—as also supported by a large body of genetic and biochemical evidence for the SMXL6 protein in general (Soundappan et al., 2015; Wang et al., 2015; Samodelov et al., 2016).

Contradicting the previous conclusion that the D2 domain of a SMXL/D53 protein in rice is sufficient for protein interaction with D14 and for proteasomal degradation (Shabek et al., 2018), exclusively the D1M domain of the Arabidopsis

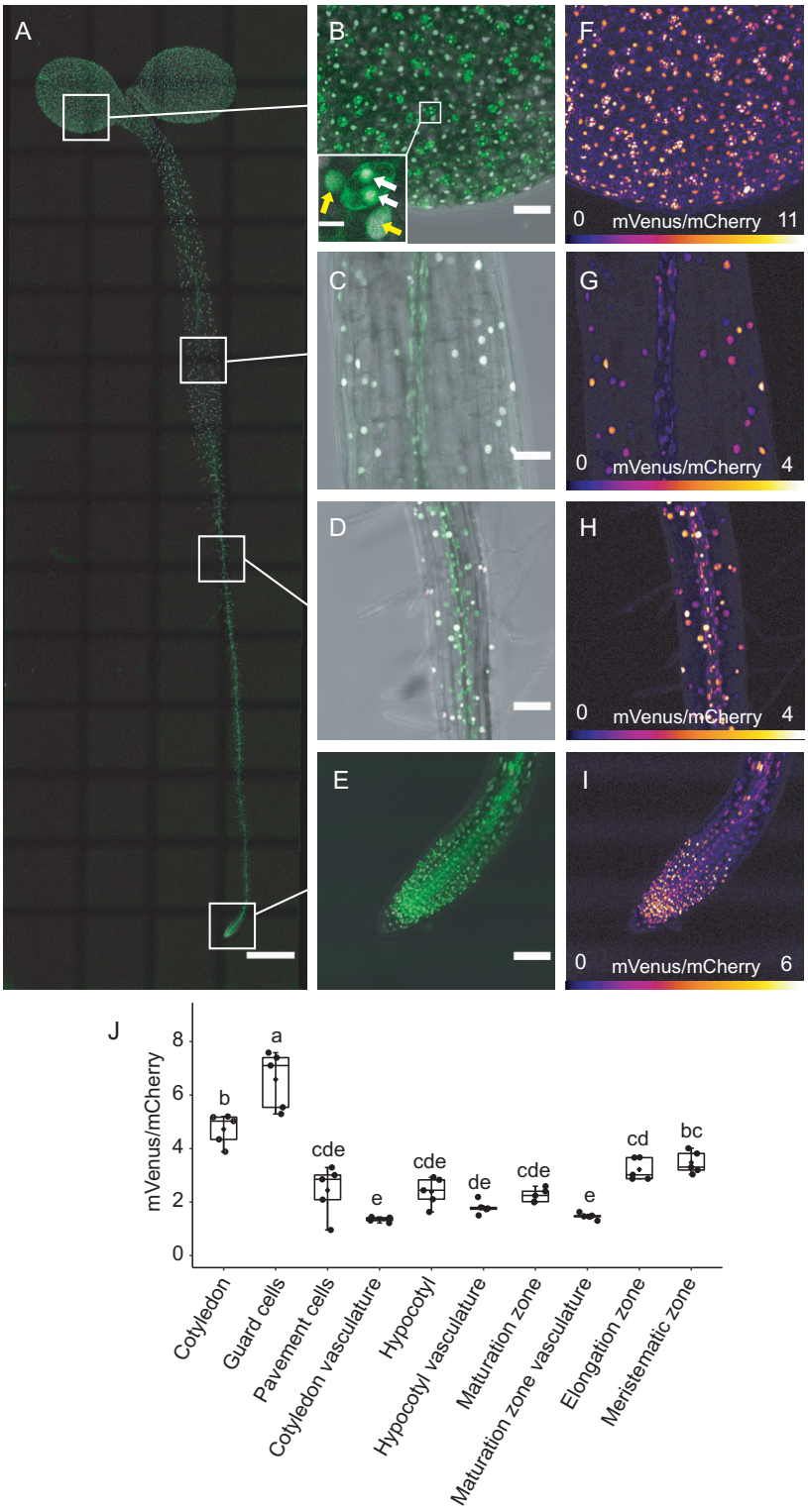

Figure 4 Expression of Strigo-D2 in Arabidopsis seedlings. A, Ubiquitous activity of Strigo-D2. Shown are overlays of mVenus and mCherry-derived signals. Green: mVenus. Magenta: mCherry. Scale bar: 500 μm. B–E, Activity of Strigo-D2 in cotyledons (B), hypocotyls (C), root maturation zones (D), and root tips (E). Images were recaptured from the positions indicated in (A) with higher magnification. Shown are overlays of mVenus, mCherry, and brightfield-derived signals. Green: mVenus. Magenta: mCherry. Grey: brightfield. Scale bars: 50 μm. White arrows in (B) indicate guard cells. Yellow arrows in (B) indicate pavement cells. Scale bar in the insert in (B): 10 μm. F–I, Color-coded images generated from images shown in (B–E) visualizing mVenus/mCherry ratios indicating SL signaling levels. The color scale represents the range of intensity ratios among all targeted nuclei. 95th percentile of the ratios was used as the maximum value in order to eliminate outliers. J, mVenus/mCherry signal ratios in different organs and tissues. Elements of the boxplot: center line, median; box limits, upper and lower quartiles; whiskers, values outside upper and lower quartiles; end of the whiskers, minimum and maximum. Different letters above boxes indicate statistical groups (one-way ANOVA, post hoc LSD test with Bonferroni adjustment, $P < 0.01$, $n = 5$).

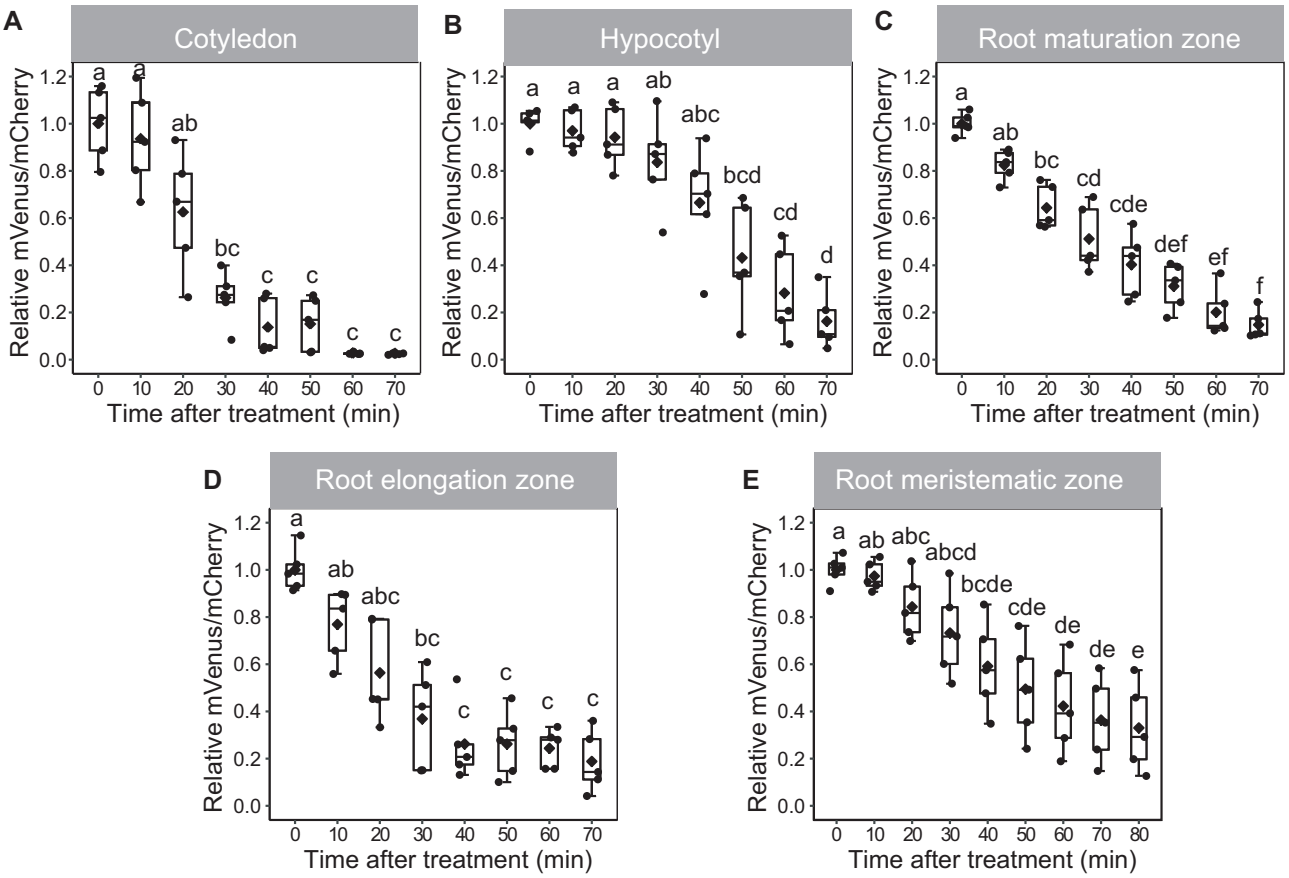

Figure 5 Strigo-D2 response to (+)-5DS treatment in different tissues. A, Cotyledons. B, Hypocotyls. C, Root maturation zones. D, Root elongation zones. E, Root meristematic zones. Concentration of (+)-5DS: 0.5 μM. Age of the plant: 4 DAG. Elements of the boxplot: center line, median; box limits, upper and lower quartiles; whiskers, values outside upper and lower quartiles; end of the whiskers, minimum and maximum. Different letters above boxes indicate statistical groups (one-way ANOVA, post hoc LSD test with Bonferroni adjustment, $P < 0.01$, $n = 5$).

SMXL7 protein interacted with D14 in yeast-based and in transient split-LUC assays (Khosla et al., 2020a). Together with the observations that D2 domains mediate homo- and heteromeric interactions between SMXL proteins and that a SMAX1-D2-LUC protein is not degraded in SMAX1/SMXL2-deficient backgrounds, these findings gave rise to the notion that isolated SMXL-D2 protein domains are only degraded due to their recruitment to SCF complexes by other full-length SMXL proteins (Khosla et al., 2020a). If true, this model would predict that Strigo-D2 activity does not only depend on the presence of the SCF-complex components D14 and MAX2 but also on the availability of endogenous SMXL proteins to interact with the expressed SMXL6-D2-mVenus fusion protein. Because *SMXL6*, *SMXL7*, and *SMXL8* promoter activities are associated with vascular tissues, which is similarly observed for *D14* and *MAX2* promoter activities (Soundappan et al., 2015; Liang et al., 2016; Shi et al., 2021), this mode of action could contribute to the observed spatial pattern of Strigo-D2 activity with a minimum mVenus/mCherry ratio around the vasculature. However, because the formation of SMXL homo- and heteromers may, according to this concept, contribute to natural SL signaling, Strigo-D2 has the potential to report also on this aspect of the process. In addition, because isolated D2 domains interact with D14 at least in vitro in an SL-dependent fashion (Shabek et al., 2018), a weak SL-triggered interaction of SMXL6-D2 with an $SCF^{MAX2/D14}$ complex may already be sufficient to induce degradation without requiring interaction with other SMXL proteins. Moreover, as indicated by the severely altered phenotype of *p35S:SMXL6-mVenus_p35S:mCherry-NLS* plants, including the D1M domain into sensor construction may interfere with endogenous SL signaling events, making the interpretation of sensor output difficult.

Independent from the mechanisms determining Strigo-D2 levels, we observed that Strigo-D2 responds to exogenous SL analogs, without exception, in all cell types investigated. Considering the very local activity of some promoter reporters monitoring expression of genes encoding SL signaling components (this study; Stirnberg et al., 2007; Chevalier et al., 2014), this finding is remarkable as it suggests that, although to a different extent, all cells hold the potential for SL perception and signaling. With the caveat of the limitations of unraveling gene expression through promoter reporters, this means that expression of signaling components at low levels is sufficient or, as suggested previously for D14 (Chevalier et al., 2014), that SL signaling components travel at least short distances. Further investigation is required to determine the extent to which this holds true;

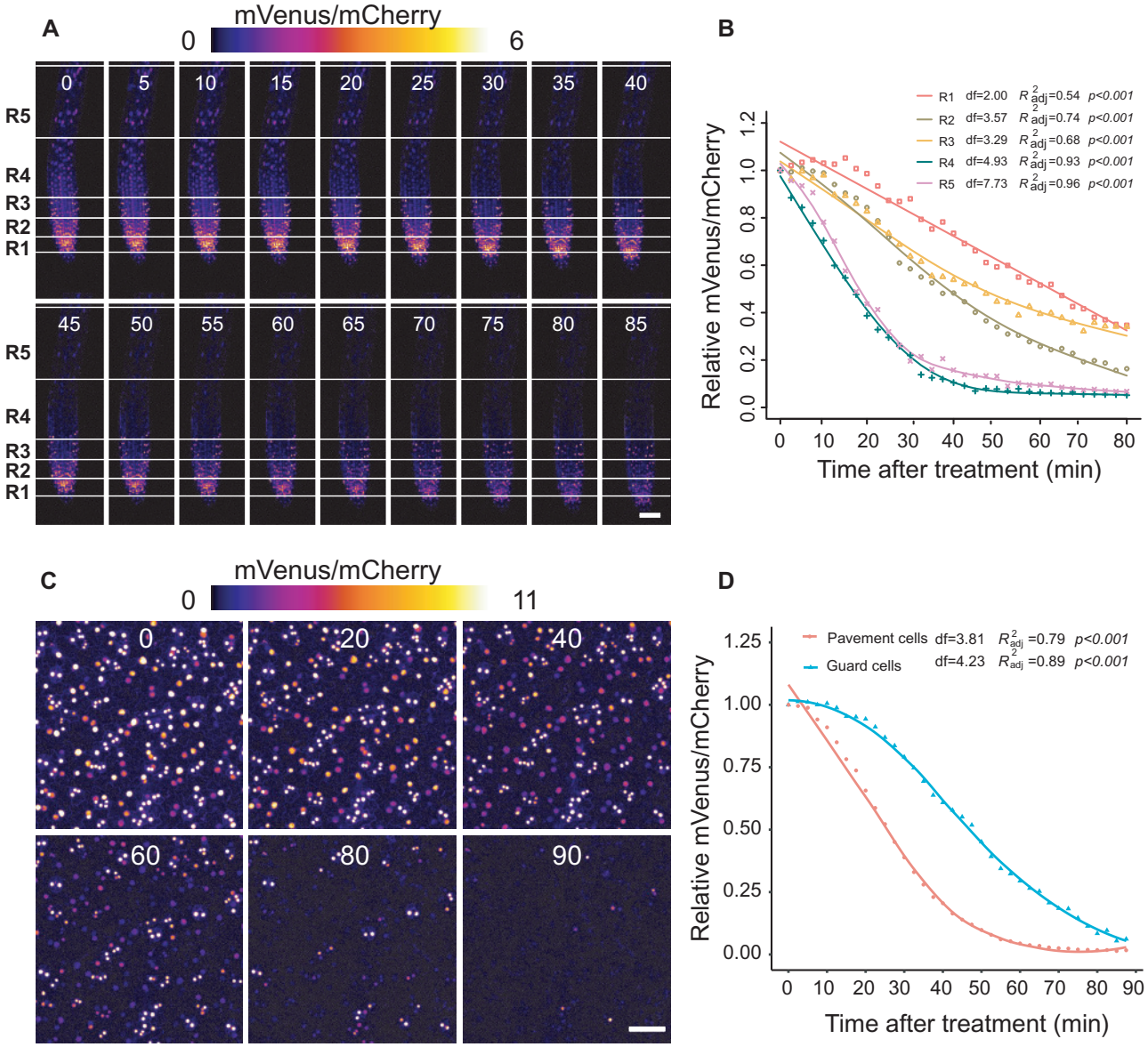

Figure 6 Strigo-D2 response to (+)-5DS at a cellular resolution in root tips and cotyledon epidermis. A, Color-coded images of root tips generated from confocal images at the indicated time points (in minutes, shown above each image) after application. Concentration of (+)-5DS: 0.5 μM. Covered range of the regions (distance from bottom of meristematic zone): R1: 0–65 μm, R2: 65–130 μm, R3: 130–195 μm, R4: 195–395 μm, R5: 395–595 μm. Scale bar: 50 μm. B, Dynamics of mVenus/mCherry ratios in four regions of the root tip after application. $n = 3$. C, Color-coded images representing mVenus/mCherry signal ratios in the cotyledon epidermis at indicated time points (in minutes, shown above each image) after application. Concentration of (+)-5DS: 0.5 μM. Scale bar: 50 μm. D, Dynamics of mVenus/mCherry ratios in pavement and guard cells. $n = 3$. Curves in (B and D) were generated by non-linear regression and computed in R using the ss Function in the npreg Package. df: degree of freedom. Data points are mean values of three biological replicates. Adjusted R^2 indicates how well generated curves fit obtained data points. *P*-values for the *F* test indicate significance levels of the correlation between the models and obtained data. The null hypothesis to be rejected is that the parameter effect (time) equals zero.

in this study, guard cells showed no *MAX2* reporter activity and a low but nonetheless very clear response. Considering that the expression of SMXL target proteins also seems to be rather spatially restricted (Soundappan et al., 2015; Liang et al., 2016), the question emerges whether a ubiquitous SL signaling capacity is indeed relevant and whether distinct SL responses are based on local or systemic effects. The recent identification of the direct transcriptional targets of SMXL6, SMXL7, and SMXL8 proteins (Wang et al., 2020) allows the analysis of target activity in respective mutants, likewise with cellular resolution, and thereby addresses this aspect. In fact, combination of the Strigo-D2 sensor with transcriptional reporters revealing target gene activity has the potential to reveal associations between signaling and signaling output. Establishment of a förster resonance energy transfer (FRET)-based direct sensor for SL molecules, as for example generated for gibberellins by employing the α/β-hydrolase-like receptor GIBBERELLIN INSENSITIVE DWARF 1A (Rizza et al., 2017), will complete the toolbox for revealing the

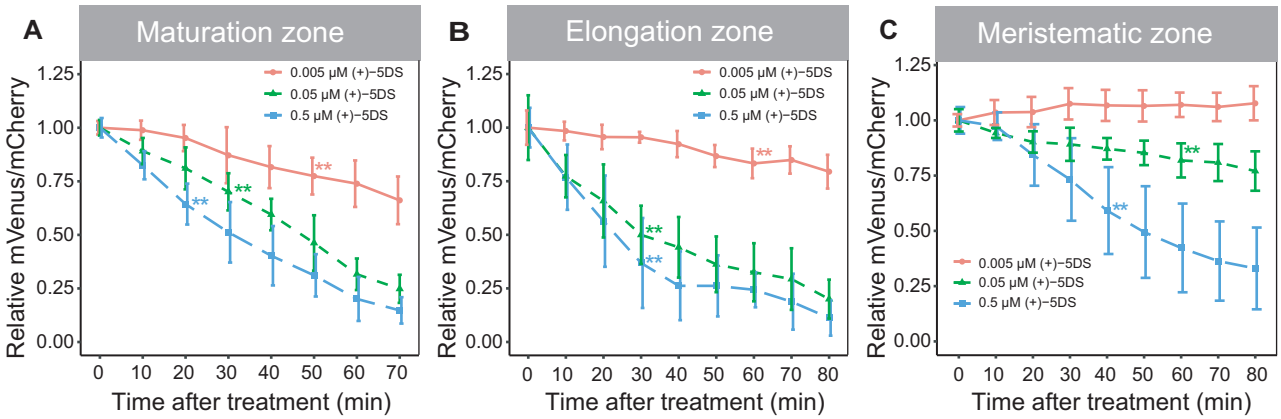

Figure 7 Sensitivity of Strigo-D2 to different (+)-5DS concentrations in the root. A, Maturation zone. B, Elongation zone. C, Meristematic zone. Asterisks indicate the first time point of significant reduction of mVenus/mCherry ratios compared to before the treatment as determined by one-way ANOVA, post hoc LSD test with Bonferroni adjustment, $P < 0.01$. $n = 5$.

whole of the spatio-temporal complexity of the SL signaling process.

Importantly, different Strigo-D2 activities in different cell types argue for differences in the capacity of cells to respond to SLs. In our study, guard cells were on one end and vascular cells on the other end of the spectrum in this regard. In light of the reported role of SL signaling in increasing drought tolerance (Haider et al., 2018; Li et al., 2020a, 2020b) and the importance of long-distance transport of SL-related molecules possible along the vasculature (Kohlen et al., 2011), the relevance of these differences and their effect on distinct cell types is certainly interesting to investigate. Moreover, identifying factors limiting SL responsiveness in individual cells may provide a means to modulate SL-dependent processes in a more targeted fashion. In guard cells, for example, we observed D14 but no MAX2 reporter activity prompting the question of whether the absence of MAX2 causes a reduced response in this specific cell type. Considering its specificity and sensitivity toward SL signaling, the Strigo-D2 sensor may be useful for addressing this question. Another example for sensor utility may be the establishment of computational models for SL signaling patterns based on dynamic sensor outputs as done previously for gibberellin (Rizza et al., 2021). Overall, we assume that the dynamic nature of Strigo-D2 will facilitate quantitative determination of SL signaling for developing a deeper understanding of SL biology.

Materials and methods

Plasmid construction

All constructs were generated via GreenGate cloning (Lampropoulos et al., 2013) if not mentioned otherwise. Used modules and primers are described in Supplemental Tables S1 and S2. Entry modules generated in this study were described as below. Three serial and partial fragments of the *SMXL6* coding sequence were amplified from cDNA with the primer pairs *SMXL6-1st-F* and *SMXL6-1st-R*, *SMXL6-2nd-F* and *SMXL6-2nd-R*, *SMXL6-3rd-F* and *SMXL6-3rd-R* to edit the endogenous Eco31I (BsaI) sites without altering the correspondent amino acid sequence. After digestion with Eco31I, the purified products were ligated into *pGGC000* (Lampropoulos et al., 2013). We used the In-Fusion (Takara Bio) system to obtain the full-length *SMXL6* cDNA from these partial vectors with the following primer pairs (*E2-5-bp-deletion-F* and *E2-5-bp-deletion-R*, *SMXL6-frag1-into-E2-F* and *SMXL6-frag1-into-E2-R*). The *SMXL6-D2* fragment was cloned using primer pair *SMXL6-D2-F* and *SMXL6-3rd-R*. *D14* and *MAX2* promoters were amplified by primers described in Supplemental Table S2 and cloned into *pGGA000* (Lampropoulos et al., 2013). Entry modules with abovementioned desired fragments were subsequently cloned into intermediate modules using *pGGM000* by GreenGate reaction (Lampropoulos et al., 2013), and intermediate modules were finally transferred into destination vector *pGGZ000* (Lampropoulos et al., 2013; Schürholz et al., 2018; Wallner et al., 2019) via another GreenGate reaction.

Plant material and generation of transgenic lines

In this study, the Arabidopsis (*A. thaliana*) Col-0 ecotype was used as genetic background. Loss-of-function alleles of *D14* (*d14-1*: WiscDsLoxHs137_07E) and *KAI2* (*htl-3*: 15-bp deletion [Toh et al., 2014]) were obtained from David Nelson (UC Riverside, USA). Plants were transformed using an *Agrobacterium tumefaciens*-based floral-dip method to obtain transgenic lines.

Plant growth condition

Seeds were surface-sterilized in a 1.5-mL microcentrifuge tubes with 700 µL of washing solution (70% v/v ethanol in water, 0.1% v/v tween-20) by incubating in 37°C shaker (200 rpm) for 10 min, then washed five times with dH20 in the clean bench. Afterwards, seeds were stratified in 500 µL of dH_2O at 4°C in the dark for 3 d and sown on plates with 0.8% w/v agar in 1/2 Murashige and Skoog (MS) medium supplemented with 1% w/v sucrose and grown vertically. Seedlings used for microscopic or phenotypic analysis were grown vertically in short-day conditions (10-h light and 14-h

darkness) at 21°C. For microscopic analysis, seedlings were grown for 4 d after being transferred to growth chamber, while this period was increased to 5 d for root phenotypic analysis. For 4-week-old plants, from the third week onwards, seedlings were grown in long day (16-h light and 8-h dark) conditions at 21°C. For the independent transgenic lines in WT background, only lines with single integration based on T2 segregation ratios were propagated to T3, and lines homozygous for the Basta resistance were selected for characterization.

Chemicals and treatments

The SL substrates (+)-5-deoxy-strigol [(+)-5DS, CAS No: 151716-18-6] was obtained from OlChemIm Ltd (Olomouc, Czech Republic), (±)-GR24 (*rac*-GR24, CAS No: 76974-79-3), and Karrikin1 (KAR1, CAS No: 857054-02-5) were purchased from Chiralix (Nijmegen, Netherland). $GR24^{4DO}$ was obtained from StrigoLab (Torino, Italy). IAA (CAS No: 87-51-4), trans-Zeatin (Cytokinin, CK, CAS No: 1637-39-4), (±)-ABA (CAS No:14375-45-2), and GA_3 (CAS No: 77-06-5) were purchased from Merck KGaA/Sigma-Aldrich (Darmstadt, Germany). For generating stock solutions, (+)-5DS, *rac*-GR24, KAR1, and $GR24^{4DO}$ were dissolved in acetone, IAA, CK, and ABA were dissolved in 1-N NaOH and GA_3 was dissolved in ethanol before diluted with water to reach stock concentrations. All hormone and mock solutions were then diluted with 1/2 MS medium to working concentrations. The same working concentration of 0.5 μM was applied for (+)-5DS, *rac*-GR24, KAR1, and $GR24^{4DO}$ if not stated otherwise and as used previously (Scaffidi et al., 2014; Samodelov et al., 2016; Villaécija-Aguilar et al., 2019; Khosla et al., 2020a; Wang et al., 2020). Working concentrations for IAA, CK, ABA, and GA_3 were 1, 5, 2, and 5 μM, respectively, as applied previously (Waadt et al., 2014; Liao et al., 2015; Osugi et al., 2017; Rizza et al., 2021). Five 4-d-old seedlings were transferred from 1/2 MS plates onto a chambered coverslip (Cat. No:80286, ibidi GmbH, Gräfelfing, Germany) containing 120-μL treatment solution. The seedlings were immersed in solution and covered by a piece of fabric mesh. Then the slide chamber was covered with lid to avoid evaporation.

Preparation for time-lapse imaging

Four-day-old seedling were transferred onto a chambered coverslip containing 60 μL 1/2 MS medium, covered by a piece of mesh, and fixed by an adjusted paper clip to avoid movement. The slide chamber was covered by a glass slide and sealed with water to avoid evaporation. Afterwards, the position of interest on the seedling was marked under the microscope and an image for time-point zero (t0) was acquired. Then, 60 μL of (+)-5DS was added through the mesh and mixed with the 1/2 MS medium by gently pipetting and recording was started immediately. Focus was adjusted before the first timepoint of time-lapse imaging t1 and the time-lapse imaging was started from t1. Effect of different concentrations was monitored in root maturation zones, elongation zones, and meristematic zones using final concentrations of 0.5-, 0.05-, and 0.005-μM (+)-5DS.

Image acquisition and analysis

Bright field and fluorescence images were acquired using a Leica TCS SP8 confocal microscope (Leica Microsystems, Wetzlar, Germany), mVenus was excited by 514-nm laser light, while mCherry was excited using 561 nm. Emissions were detected sequentially to avoid cross-talk between fluorophores. mVenus and mCherry fluorescence were detected in the range of 524–540 nm and 571–630 nm, respectively. The cyan fluorescent protein in *D14* and *MAX2* reporter lines was excited by 458 nm laser light and detected in the range of 465–509 nm. The YFP in the SMAX1-YFP reporter line was excited by 514-nm laser light and detected in the range of 524–540 nm. The output power of the 514-nm laser was set to 30%. For imaging of seedlings expressing SMXL6-D2-mVenus and mCherry-NLS, the intensity of 514-nm and 561-nm lasers were consistently set to 1.0% and 0.04%, respectively. While for imaging of seedlings expressing SMXL6-mVenus and mCherry-NLS, the intensity of 514-nm and 561-nm lasers were consistently set at 10% and 0.04%, respectively. Tile scanning of whole seedlings was performed using a 10× objective, while other images were acquired using a HC PL APO 20x/0.75 IMM objective. Z-stacks covering the entire thickness of observed tissue were acquired. Step size for tile scanning was 10 μm and that for other image acquisitions was 5 μm. Images were analyzed using Fiji (Schindelin et al., 2012). Maturation, elongation, and meristematic zones of roots were defined as previously described (Waadt et al., 2014). For determining root length, plates were scanned by an Epson Perfection V600 Photo scanner and measured in Fiji using the freehand line tool. Composite images containing mVenus and mCherry channel information were generated by Fiji and automatically processed and analyzed using macro codes. For image stacks, Z projections using the "maximum projection" option were performed. Composite images with multiple frames (generated from time-lapse imaging) were saved as image sequence before intensity measurements. To measure fluorescence intensity in each individual channel, proper intensity thresholds were set depending on the targeted cell type to eliminate noise from auto-fluorescence. The "Watershed" function was applied to separate crowded nuclei. Afterwards, nuclei were sampled and measured using the "Analyze Particles" tool for each time point and each channel separately. For images containing different types of cells, the "freehand" tool was used to select regions of specific cells. Fluorescence intensity of each nucleus was determined using gray values collected in the respective channels. Fluorescence intensity ratio of each nucleus was calculated in Excel (Microsoft, Redmont, USA) by dividing the values of mVenus by the values of mCherry. The mean value of all nuclei in the same frame was taken as one biological repetition. Relative fluorescence intensity ratio references the average ratio at time 0 min or to the mock, respectively. The same method was applied for all images of each analysis. False color images were generated by "Calculator Plus" in Fiji through calculating intensity ratios of each pixel from mVenus and mCherry channels after being Gaussian Blurred and subtracting background. Color

scale was calculated based on the range of intensity ratios of all the nuclei. The 95th percentile of the ratios was used as the maximum value in order to eliminate outliers. One-way analysis of variance was conducted using R, statistical significance among data sets was calculated using the post hoc LSD test with Bonferroni adjustment. Spline regression was used for estimating function of response curves. Curves of best fit were computed in R using ss Function in the npreg Package (Helwig, 2020). Charts were generated in R using ggplot2 (Villanueva and Chen, 2019).

Accession numbers

Sequence data from this article can be found in the GenBank/EMBL data libraries under the following accession numbers. SMXL6: NP_001077474/AT1G07200; D14: NP_566220/AT3G03990; MAX2: NP_565979/AT2G42620; KAI2: NP_195463/AT4G37470.

Supplemental data

The following materials are available in the online version of this article.

Supplemental Figure S1. Comparison of fluorescent signals in transgenic seedlings carrying Strigo-D2 or *p35S:SMXL6-mVenus_p35S:mCherry-NLSs* transgenes.

Supplemental Figure S2. Effect of SLs and KAR1 on Strigo-D2 in the root maturation zone of different genetic backgrounds.

Supplemental Figure S3. Effect of SLs and KAR1 on *pSMXL5:SMAX1-YFP* reporter activity.

Supplemental Figure S4. Strigo-D2 response to (+)-5DS and other plant hormones in the root maturation zone.

Supplemental Figure S5. Strigo-D2 activity in seedlings.

Supplemental Figure S6. Strigo-D2 activity in the vasculature of cotyledons, hypocotyls and root maturation zones.

Supplemental Figure S7. *D14* and *MAX2* promoter reporter activity in seedlings.

Supplemental Figure S8. Spline regression of relative mVenus/mCherry as function of treatment time in different tissues.

Supplemental Figure S9. Dual-channel representation of Strigo-D2 response to (+)-5DS at a cellular resolution in root tips and cotyledon epidermis.

Supplemental Figure S10. Spline regression of relative mVenus/mCherry as function of treatment time under gradient (+)-5DS concentrations in different zones of the root.

Supplemental Table S1. GreenGate vectors used in this study.

Supplemental Table S2. Primers used in this study.

Supplemental Movie 1. Strigo-D2 response to (+)-5DS treatment in cotyledons.

Supplemental Movie 2. Strigo-D2 response to (+)-5DS treatment in hypocotyls.

Supplemental Movie 3. Strigo-D2 response to (+)-5DS treatment in root maturation zones.

Supplemental Movie 4. Strigo-D2 response to (+)-5DS treatment in root tips.

Supplemental Movie 5. Gradual decrease of Strigo-D2 responsiveness from the maturation zone to the very tip of the root.

Supplemental Movie 6. Strigo-D2 shows a faster response to (+)-5DS in pavement cells than in guard cells.

Funding

This work was supported by a fellowship of the Chinese Scholarship Council (CSC) and a Peterson scholarship (http://www.peterson-elites.sdu.edu.cn/jxjjj.htm) to J.Z., a European Research Council (ERC) Consolidator grant [647148, PLANTSTEMS] and a grant of the Deutsche Forschungsgemeinschaft [DFG, GR_2104/4-1] to T.G., by funds of the DFG [GR4559_4-1, GR4559_5-1 and EXC-2048/1 – project ID 390686111] to G.G., and postdoctoral fellowships of the Alexander von Humboldt-Stiftung [3.5-JPN – 1164674-HFST-P] and the Japan Society for the Promotion of Science [JSPS Overseas Research Fellowships 201960008] to D.S. We thank the Nikon Imaging Center (NIC) of Heidelberg University for support and Annika Guse (COS, Heidelberg) for access to confocal microscopes.

Conflict of interest statement. None declared.

References

Akiyama K, Matsuzaki K-i, Hayashi H (2005) Plant sesquiterpenes induce hyphal branching in arbuscular mycorrhizal fungi. Nature **435**: 824–827

Al-Babili S, Bouwmeester HJ (2015) Strigolactones, a novel carotenoid-derived plant hormone. Annu Rev Plant Biol **66**: 161–186

Alder A, Jamil M, Marzorati M, Bruno M, Vermathen M, Bigler P, Ghisla S, Bouwmeester H, Beyer P, Al-Babili S (2012) The path from β-carotene to carlactone, a strigolactone-like plant hormone. Science **335**: 1348–1351

Arite T, Umehara M, Ishikawa S, Hanada A, Maekawa M, Yamaguchi S, Kyozuka J (2009) d14, a strigolactone-insensitive mutant of rice, shows an accelerated outgrowth of tillers. Plant Cell Physiol **50**: 1416–1424

Benfey PN, Chua NH (1990) The cauliflower mosaic virus 35S promoter: combinatorial regulation of transcription in plants. Science **250**: 959–966

Bennett T, Liang Y, Seale M, Ward S, Müller D, Leyser O (2016) Strigolactone regulates shoot development through a core signalling pathway. Biol Open **5**: 1806–1820

Booker J, Sieberer T, Wright W, Williamson L, Willett B, Stirnberg P, Turnbull C, Srinivasan M, Goddard P, Leyser O (2005) MAX1 encodes a cytochrome P450 family member that acts downstream of MAX3/4 to produce a carotenoid-derived branch-inhibiting hormone. Dev Cell **8**: 443–449

Braguy J, Samodelov SL, Andres J, Ochoa-Fernandez R, Al-Babili S, Zurbriggen MD (2021) A protoplast-based bioassay to quantify strigolactone activity in Arabidopsis using StrigoQuant. Methods Mol Biol **2309**: 201–218

Brewer PB, Yoneyama K, Filardo F, Meyers E, Scaffidi A, Frickey T, Akiyama K, Seto Y, Dun EA, Cremer JE (2016) LATERAL BRANCHING OXIDOREDUCTASE acts in the final stages of strigolactone biosynthesis in Arabidopsis. Proc Natl Acad Sci USA **113**: 6301–6306

Chesterfield RJ, Vickers CE, Beveridge CA (2020) Translation of strigolactones from plant hormone to agriculture: achievements, future perspectives, and challenges. Trends Plant Sci **25**: 1087–1106

Chevalier F, Nieminen K, Sánchez-Ferrero JC, Rodríguez ML, Chagoyen M, Hardtke CS, Cubas P (2014) Strigolactone promotes degradation of DWARF14, an α/β hydrolase essential for strigolactone signaling in Arabidopsis. Plant Cell **26**: 1134–1150

Conn CE, Nelson DC (2015) Evidence that KARRIKIN-INSENSITIVE2 (KAI2) receptors may perceive an unknown signal that is not karrikin or strigolactone. Front Plant Sci **6**: 1219

Cook C, Whichard LP, Turner B, Wall ME, Egley GH (1966) Germination of witchweed (Striga lutea Lour.): isolation and properties of a potent stimulant. Science **154**: 1189–1190

Domagalska MA, Leyser O (2011) Signal integration in the control of shoot branching. Nat Rev Mol Cell Biol **12**: 211–221

Fehr M, Frommer WB, Lalonde S (2002) Visualization of maltose uptake in living yeast cells by fluorescent nanosensors. Proc Natl Acad Sci USA **99**: 9846–9851

Flematti GR, Scaffidi A, Waters MT, Smith SM (2016) Stereospecificity in strigolactone biosynthesis and perception. Planta **243**: 1361–1373

Gomez-Roldan V, Fermas S, Brewer PB, Puech-Pagès V, Dun EA, Pillot J-P, Letisse F, Matusova R, Danoun S, Portais J-C (2008) Strigolactone inhibition of shoot branching. Nature **455**: 189–194

Haider I, Andreo-Jimenez B, Bruno M, Bimbo A, Floková K, Abuauf H, Ntui VO, Guo X, Charnikhova T, Al-Babili S, et al. (2018) The interaction of strigolactones with abscisic acid during the drought response in rice. J Exp Bot **69**: 2403–2414

Helwig NE (2020) Multiple and Generalized Nonparametric Regression. SAGE, London

Isoda R, Yoshinari A, Ishikawa Y, Sadoine M, Simon R, Frommer WB, Nakamura M (2021) Sensors for the quantification, localization and analysis of the dynamics of plant hormones. Plant J **105**: 542–557

Jiang L, Liu X, Xiong G, Liu H, Chen F, Wang L, Meng X, Liu G, Yu H, Yuan Y (2013) DWARF 53 acts as a repressor of strigolactone signalling in rice. Nature **504**: 401–405

Khosla A, Morffy N, Li Q, Faure L, Chang SH, Yao J, Zheng J, Cai ML, Stanga J, Flematti GR (2020a) Structure–function analysis of SMAX1 reveals domains that mediate its karrikin-induced proteolysis and interaction with the receptor KAI2. Plant Cell **32**: 2639–2659

Khosla A, Rodriguez-Furlan C, Kapoor S, Van Norman JM, Nelson DC (2020b) A series of dual-reporter vectors for ratiometric analysis of protein abundance in plants. Plant Direct **4**: e00231

Kohlen W, Charnikhova T, Liu Q, Bours R, Domagalska MA, Beguerie S, Verstappen F, Leyser O, Bouwmeester H, Ruyter-Spira C (2011) Strigolactones are transported through the xylem and play a key role in shoot architectural response to phosphate deficiency in nonarbuscular mycorrhizal host Arabidopsis. Plant Physiol **155**: 974–987

Kremers GJ, Goedhart J, van Munster EB, Gadella TW Jr. (2006) Cyan and yellow super fluorescent proteins with improved brightness, protein folding, and FRET Förster radius. Biochemistry **45**: 6570–6580

Lampropoulos A, Sutikovic Z, Wenzl C, Maegele I, Lohmann JU, Forner J (2013) GreenGate-a novel, versatile, and efficient cloning system for plant transgenesis. PloS One **8**: e83043

Larrieu A, Champion A, Legrand J, Lavenus J, Mast D, Brunoud G, Oh J, Guyomarc'h S, Pizot M, Farmer EE (2015) A fluorescent hormone biosensor reveals the dynamics of jasmonate signalling in plants. Nature Commun **6**: 1–9

Li S, Chen L, Li Y, Yao R, Wang F, Yang M, Gu M, Nan F, Xie D, Yan J (2016) Effect of GR24 stereoisomers on plant development in Arabidopsis. Mol Plant **9**: 1432–1435

Li W, Nguyen KH, Chu HD, Watanabe Y, Osakabe Y, Sato M, Toyooka K, Seo M, Tian L, Tian C, et al. (2020a) Comparative functional analyses of DWARF14 and KARRIKIN INSENSITIVE 2 in drought adaptation of Arabidopsis thaliana. Plant J **103**: 111–127

Li W, Nguyen KH, Tran CD, Watanabe Y, Tian C, Yin X, Li K, Yang Y, Guo J, Miao Y, et al. (2020b) Negative roles of strigolactone-related SMXL6, 7 and 8 proteins in drought resistance in Arabidopsis. Biomolecules **10**: 607

Liang Y, Ward S, Li P, Bennett T, Leyser O (2016) SMAX1-LIKE7 signals from the nucleus to regulate shoot development in Arabidopsis via partially EAR motif-independent mechanisms. Plant Cell **28**: 1581–1601

Liao C-Y, Smet W, Brunoud G, Yoshida S, Vernoux T, Weijers D (2015) Reporters for sensitive and quantitative measurement of auxin response. Nat Methods **12**: 207–210

Miyawaki A, Llopis J, Heim R, McCaffery JM, Adams JA, Ikura M, Tsien RY (1997) Fluorescent indicators for Ca 2 + based on green fluorescent proteins and calmodulin. Nature **388**: 882–887

Moturu TR, Thula S, Singh RK, Nodzynski T, Vareková RS, Friml J, Simon S (2018) Molecular evolution and diversification of the SMXL gene family. J Exp Bot **69**: 2367–2378

Osugi A, Kojima M, Takebayashi Y, Ueda N, Kiba T, Sakakibara H (2017) Systemic transport of trans-zeatin and its precursor have differing roles in Arabidopsis shoots. Nat Plants **3**: 17112

Rizza A, Tang B, Stanley CE, Grossmann G, Owen MR, Band LR, Jones AM (2021) Differential biosynthesis and cellular permeability explain longitudinal gibberellin gradients in growing roots. Proc Natl Acad Sci USA **118**: e1921960118

Rizza A, Walia A, Lanquar V, Frommer WB, Jones AM (2017) In vivo gibberellin gradients visualized in rapidly elongating tissues. Nat Plants **3**: 803–813

Ruyter-Spira C, Al-Babili S, Van Der Krol S, Bouwmeester H (2013) The biology of strigolactones. Trends Plant Sci **18**: 72–83

Samodelov SL, Beyer HM, Guo X, Augustin M, Jia KP, Baz L, Ebenhöh O, Beyer P, Weber W, Al-Babili S, et al. (2016) StrigoQuant: a genetically encoded biosensor for quantifying strigolactone activity and specificity. Sci Adv **2**: e1601266

Scaffidi A, Waters MT, Sun YK, Skelton BW, Dixon KW, Ghisalberti EL, Flematti GR, Smith SM (2014) Strigolactone hormones and their stereoisomers signal through two related receptor proteins to induce different physiological responses in Arabidopsis. Plant Physiol **165**: 1221–1232

Schindelin J, Arganda-Carreras I, Frise E, Kaynig V, Longair M, Pietzsch T, Preibisch S, Rueden C, Saalfeld S, Schmid B (2012) Fiji: an open-source platform for biological-image analysis. Nat Methods **9**: 676–682

Schürholz AK, López-Salmerón V, Li Z, Forner J, Wenzl C, Gaillochet C, Augustin S, Barro AV, Fuchs M, Gebert M, et al. (2018) A comprehensive toolkit for inducible, cell type-specific gene expression in Arabidopsis. Plant Physiol **178**: 40–53

Seto Y, Sado A, Asami K, Hanada A, Umehara M, Akiyama K, Yamaguchi S (2014) Carlactone is an endogenous biosynthetic precursor for strigolactones. Proc Natl Acad Sci USA **111**: 1640–1645

Seto Y, Yasui R, Kameoka H, Tamiru M, Cao M, Terauchi R, Sakurada A, Hirano R, Kisugi T, Hanada A (2019) Strigolactone perception and deactivation by a hydrolase receptor DWARF14. Nat Commun **10**: 1–10

Shabek N, Ticchiarelli F, Mao H, Hinds TR, Leyser O, Zheng N (2018) Structural plasticity of D3–D14 ubiquitin ligase in strigolactone signalling. Nature **563**: 652–656

Shaner NC, Campbell RE, Steinbach PA, Giepmans BN, Palmer AE, Tsien RY (2004) Improved monomeric red, orange and yellow fluorescent proteins derived from Discosoma sp. red fluorescent protein. Nat Biotechnol **22**: 1567–1572

Shen H, Luong P, Huq E (2007) The F-box protein MAX2 functions as a positive regulator of photomorphogenesis in Arabidopsis. Plant Physiol **145**: 1471–1483

Shi D, Jouannet V, Agustí J, Kaul V, Levitsky V, Sanchez P, Mironova VV, Greb T (2021) Tissue-specific transcriptome profiling of the Arabidopsis inflorescence stem reveals local cellular signatures. Plant Cell **33**: 200–223

Soundappan I, Bennett T, Morffy N, Liang Y, Stanga JP, Abbas A, Leyser O, Nelson DC (2015) SMAX1-LIKE/D53 family members

enable distinct MAX2-dependent responses to strigolactones and karrikins in Arabidopsis. Plant Cell **27**: 3143–3159

Stanga JP, Morffy N, Nelson DC (2016) Functional redundancy in the control of seedling growth by the karrikin signaling pathway. Planta **243**: 1397–1406

Stirnberg P, Furner IJ, Ottoline Leyser H (2007) MAX2 participates in an SCF complex which acts locally at the node to suppress shoot branching. Plant J **50**: 80–94

Takanaga H, Chaudhuri B, Frommer WB (2008) GLUT1 and GLUT9 as major contributors to glucose influx in HepG2 cells identified by a high sensitivity intramolecular FRET glucose sensor. Biochim Biophys Acta **1778**: 1091–1099

Toh S, Holbrook-Smith D, Stokes ME, Tsuchiya Y, McCourt P (2014) Detection of parasitic plant suicide germination compounds using a high-throughput Arabidopsis HTL/KAI2 strigolactone perception system. Chem Biol **21**: 988–998

Uslu VV, Grossmann G (2016) The biosensor toolbox for plant developmental biology. Curr Opin Plant Biol **29**: 138–147

Villaécija-Aguilar JA, Hamon-Josse M, Carbonnel S, Kretschmar A, Schmid C, Dawid C, Bennett T, Gutjahr C (2019) SMAX1/SMXL2 regulate root and root hair development downstream of KAI2-mediated signalling in Arabidopsis. PLoS Genetics **15**: e1008327

Villanueva RAM, Chen ZJ (2019) ggplot2: Elegant Graphics for Data Analysis. Taylor & Francis, New York

Waadt R, Hitomi K, Nishimura N, Hitomi C, Adams SR, Getzoff ED, Schroeder JI (2014) FRET-based reporters for the direct visualization of abscisic acid concentration changes and distribution in Arabidopsis. eLife **3**: e01739

Wallner E-S, López-Salmerón V, Belevich I, Poschet G, Jung I, Grünwald K, Sevilem I, Jokitalo E, Hell R, Helariutta Y (2017) Strigolactone-and karrikin-independent SMXL proteins are central regulators of phloem formation. Curr Biol **27**: 1241–1247

Wallner E-S, Tonn N, Wanke F, Lopéz-Salmerón V, Gebert M, Wenzl C, Lohmann JU, Harter K, Greb T (2019) OBERON3 and SUPPRESSOR OF MAX2 1-LIKE proteins form a regulatory module specifying phloem identity. bioRxiv. DOI: 10.1101/2019.12.21.885863

Wang L, Wang B, Jiang L, Liu X, Li X, Lu Z, Meng X, Wang Y, Smith SM, Li J (2015) Strigolactone signaling in Arabidopsis regulates shoot development by targeting D53-like SMXL repressor proteins for ubiquitination and degradation. Plant Cell **27**: 3128–3142

Wang L, Wang B, Jiang L, Liu X, Li X, Lu Z, Meng X, Wang Y, Smith SM, Li J (2015) Strigolactone signaling in Arabidopsis regulates shoot development by targeting D53-like SMXL repressor proteins for ubiquitination and degradation. Plant Cell **27**: 3128–3142

Wang L, Wang B, Yu H, Guo H, Lin T, Kou L, Wang A, Shao N, Ma H, Xiong G (2020) Transcriptional regulation of strigolactone signalling in Arabidopsis. Nature **583**: 277–281

Wang L, Xu Q, Yu H, Ma H, Li X, Yang J, Chu J, Xie Q, Wang Y, Smith SM, et al. (2020) Strigolactone and karrikin signaling pathways elicit ubiquitination and proteolysis of SMXL2 to regulate hypocotyl elongation in Arabidopsis. Plant Cell **32**: 2251–2270

Wang Y, Bouwmeester HJ (2018) Structural diversity in the strigolactones. J Exp Bot **69**: 2219–2230

Waters MT, Gutjahr C, Bennett T, Nelson DC (2017) Strigolactone signaling and evolution. Annu Rev Plant Biol **68**: 291–322

Waters MT, Nelson DC, Scaffidi A, Flematti GR, Sun YK, Dixon KW, Smith SM (2012) Specialisation within the DWARF14 protein family confers distinct responses to karrikins and strigolactones in Arabidopsis. Development **139**: 1285–1295

Wendrich JR, Yang B, Vandamme N, Verstaen K, Smet W, Van de Velde C, Minne M, Wybouw B, Mor E, Arents HE, et al. (2020) Vascular transcription factors guide plant epidermal responses to limiting phosphate conditions. Science **370**: eaay4970

Wheeldon CD, Bennett T (2021) There and back again: an evolutionary perspective on long-distance coordination of plant growth and development. Semin Cell Dev Biol **109**: 55–67

Yang T, Lian Y, Wang C (2019) Comparing and contrasting the multiple roles of butenolide plant growth regulators: strigolactones and karrikins in plant development and adaptation to abiotic stresses. Int J Mol Sci **20**:6270

Yao R, Ming Z, Yan L, Li S, Wang F, Ma S, Yu C, Yang M, Chen L, Chen L, et al. (2016) DWARF14 is a non-canonical hormone receptor for strigolactone. Nature **536**: 469–473

Yoneyama K, Xie X, Yoneyama K, Kisugi T, Nomura T, Nakatani Y, Akiyama K, McErlean CS (2018) Which are the major players, canonical or non-canonical strigolactones? J Exp Bot **69**: 2231–2239

Zhang Y, Van Dijk AD, Scaffidi A, Flematti GR, Hofmann M, Charnikhova T, Verstappen F, Hepworth J, Van Der Krol S, Leyser O (2014) Rice cytochrome P450 MAX1 homologs catalyze distinct steps in strigolactone biosynthesis. Nat Chem Biol **10**: 1028–1033

Zhao L-H, Zhou XE, Wu Z-S, Yi W, Xu Y, Li S, Xu T-H, Liu Y, Chen R-Z, Kovach A (2013) Crystal structures of two phytohormone signal-transducing α/β hydrolases: karrikin-signaling KAI2 and strigolactone-signaling DWARF14. Cell Res **23**: 436–439

Zhou F, Lin Q, Zhu L, Ren Y, Zhou K, Shabek N, Wu F, Mao H, Dong W, Gan L (2013) D14–SCF D3-dependent degradation of D53 regulates strigolactone signalling. Nature **504**: 406–410